EFDA–JET–CP(12)06/30

V.V. Plyusnin, V.G. Kiptily, B. Bazylev, A.E. Shevelev, E.M. Khilkevitc, J. Mlynar, M. Lehnen, G. Arnoux, A. Huber, S. Jachmich, V. Riccardo, U. Kruezi, B.Alper, R.C. Pereira, A. Fernandes, C. Reux, P.C. de Vries, T.C. Hender and JET EFDA contributors

Latest Progress in Studies of Runaway Electrons in JET

Latest Progress in Studies of Runaway Electrons in JET

V.V. Plyusnin[1], V.G. Kiptily[2], B. Bazylev[3], A.E. Shevelev[4], E.M. Khilkevitc[4], J. Mlynar[5], M. Lehnen[6], G. Arnoux[2], A. Huber[6], S. Jachmich[7], V. Riccardo[2], U. Kruezi[6], B.Alper[2], R.C. Pereira[1], A. Fernandes[1], C. Reux[8], P.C. de Vries[9], T.C. Hender[2] and JET EFDA contributors*

JET-EFDA, Culham Science Centre, OX14 3DB, Abingdon, UK

[1]Instituto de Plasmas e Fusão Nuclear, Associação EURATOM-IST, Instituto Superior Tecnico, Universidade Tecnica de Lisboa, Av. Rovisco Pais, 1049-001 Lisboa, Portugal
[2]EURATOM-CCFE Fusion Association, Culham Science Centre, OX14 3DB, Abingdon, OXON, UK
[3]Karlsruhe Institute of Technology, P.O. Box 3640, D-76021 Karlsruhe, Germany
[4]A.F. Ioffe Institute of the Russian Academy of Sciences, St Petersburg, 194021, Russia
[5]Association EURATOM/IPP.CR, IPP AS CR, CZ-18200 Prague, Czech Republic
[6]Institute for Energy Research - Plasma Physics, Forschungszentrum Juelich, Association EURATOM-FZJ, Trilateral Euregio Cluster, 52425 Juelich, Germany
[7]Laboratoire de Physique des Plasmas-Laboratorium voor Plasmafysica, Association EURATOM-Belgian State, ERM/KMS, B-1000 Brussels, Belgium
[8]CEA, IRFM, F-13108 Saint-Paul-lez- Durance, France
[9]FOM institute DIFFER, Association EURATOM-FOM, P.O. Box 1207, Nieuwegein, the Netherlands;
** See annex of F. Romanelli et al, "Overview of JET Results", (24th IAEA Fusion Energy Conference, San Diego, USA (2012)).*

Preprint of Paper to be submitted for publication in Proceedings of the 24th IAEA Fusion Energy Conference (FEC2012), San Diego, USA 8th October 2012 - 13th October 2012

ABSTRACT.
The last disruption experiments in JET with plasma facing components (PFC) based on carbon-fibre composite tiles have been carried out using either Massive Gas Injection or a constant gas puff. These studies provided new data and increased the database on disruption generated runaway electrons (RE) at JET. Temporal and spatial dynamics of RE beams have been studied using inverse reconstruction of the measured hard and soft X-rays emission during RE plateaux. Energy of RE have been measured up to 15 MeV. An analysis of plasma geometry spatial dynamics and RE generation at current quench (CQ) has shown that large decrease of RE generation rate could be achieved if plasma performs fast horizontal and/or vertical motions at CQ. Analysis of the experimental data and modelling of the interaction of RE beams with PFC in JET has shown that secondary RE could be generated during the interaction of the existing RE with PFC. First operations of JET with ITERlike Wall (ILW) have shown that the new all-metal environment did not favour to RE generation at disruptions.

1. INTRODUCTION

Major disruptions are one of the critical issues for ITER operations [1-3]. Together with the excessive electromagnetic forces and heat loads major disruptions can result in the generation of the intense beams of runaway electrons (RE). Large number of disruptions in JET [4-6], TORE Supra [7] etc. resulted in the generation of RE with energies up to several tens of Mega-electron-Volts (MeV) and densities high enough to create current plateaus up to 60-70% of the pre-disruptive plasma current. Simulations of runaway process which might occur at major disruptions in ITER demonstrate the possibility of RE currents up to 10 Mega-Amperes (MA) in multi-MeV energy ranges [8-9,1-3 (and references therein)]. Simulations also show that localized interaction of such intense RE beams with surrounding surfaces inevitably will result in inacceptable thermal loads, sputtering and melting of plasma facing components (PFC) [1-3 (and references therein)]. To avoid such detrimental consequences, efficient methods for disruption mitigation and suppression of runaway generation are essential. Detailed understanding of the physics of disruption generated RE is a key issue for the development of RE suppression techniques in present day tokamaks and in ITER.

This report presents the progress in studies of disruption generated RE achieved during latest series of disruption experiments in JET with PFC based on carbon-fibre composite (CFC) tiles [5]. Data on disruptions occurring after installation of the ITER-like wall (ILW), with the beryllium as the main material, has been collected to obtain a first insight into the impact of PFC material on the processes that generate RE.

2. DIAGNOSTICS FOR MEASUREMENTS OF RE PARAMETERS

Relativistic RE interacting with background plasma, neutrals or surrounding PFC produce a bremsstrahlung hard X-ray emission (HXR) in the MeV energy range and photo-neutrons. The HXR energy should be higher than the neutron bound energy of the target nuclei ε_n, which is for deuterium – 2.2MeV, beryllium –1.7MeV, carbon – 18.7MeV, argon – 9.9MeV, nickel – 12.0MeV,

copper – 10.6MeV, tungsten – 7.4 MeV. The energy of produced photo-neutrons is $E_n = E^{HXR} - \varepsilon_n$. An extended set of JET diagnostics has been used to measure these radiations determining RE parameters such as their energy and temporal and spatial evolution [10]. For the machine protection and RE studies 5 scintillation time-resolved HXR monitors and neutron rate fission chamber monitors (^{235}U and ^{238}U) at 3 different locations operate in a current mode with 0.1 ms time resolution. The HXR emission has been measured with the set of horizontally and vertically viewing NaI(Tl), Bi_4GeO_{12} (usually referred as BGO) and LaBr3 spectrometers. The data on the spatial distribution of HXR emission sources in the plasma has been obtained with the routinely used JET neutron/gamma profile monitor. This monitor comprises two cameras, vertical and horizontal, with 9 and 10 lines of sight, respectively. Each camera has two detectors: NE213 – for neutron and HXR measurements, and CsI detector for HXR registration. The data from vertical and horizontal sets of the detectors enabled the tomography reconstruction of the runaway beam image in HXR. Numerical analysis of the measured HXR spectra provided the data on maximal energy of runaway electrons and allowed reconstructing the energy distribution of fast electrons in visible volume. Furthermore, the soft X-ray (SXR) diagnostics consisting of vertical and horizontal cameras has been used to study the RE beams spatial evolution by the tomography reconstruction.

3. DISRUPTION SCENARIOS FOR STUDIES OF RUNAWAY ELECTRONS

A series of major disruptions in JET with CFC PFCs [5] have been triggered by either Massive Gas Injection (MGI) using a fast valve (Disruption Mitigation Valve – DMV) [11] or by a slow constant puff of impurity gas. At a maximum pressure in DMV gas storage chamber up to 2.5×10^{23} particles could be injected. In the experiments the number of injected argon or neon (or their mixtures with deuterium) atoms has been varied between $(4\text{-}6)\times10^{22}$ and $(21\text{-}24)\times10^{22}$. Usually the disruption occurred 7-10ms after the DMV activation [11], while the scenario with constant gas puff required a significantly longer time (up to 500ms) to trigger the disruption. Use of pure argon in MGI led to generation of RE with the current values sometimes larger than 1MA and duration over 0.1 second for all used gas amounts in magnetic fields above 1.8 – 2T. Traces of runaway generation registered as neutron radiation bursts have been be found for argon MGI even at very low magnetic fields $B_0 =$ 1.2T [11]. No runaway generation has been observed during MGI and slow injections when both used deuterium mixtures, pure deuterium and helium. In the past a slow constant neon puff was the standard scenario at JET to generate large (~1MA) RE currents [6]. Unlike this scenario, use of pure neon in MGI resulted in much weaker RE generation [11]. Yet another difference between the influence of fast and slow scenarios on RE generation was reported in [5]. The RE plateaux and values of measured photo-neutrons and HXR in argon MGI disruptions were significantly higher than those in slow injections at similar or lower CQ rates. This paper is focused on the detailed analysis of experiments on disruption generated RE, with and without MGI, which yielded the data on the phenomenology of runaway process, energy of RE, spatial and temporal evolutions of the RE beams including their interaction with the first wall in JET.

4. DISRUPTION EVOLUTIONS DURING MGI AND CONSTANT GAS INJECTION

The sequence of events in disruptions caused by constant gas puff (slow process) is well known and its detailed phenomenological description can be found elsewhere [1-4]. The main characteristics are: after phase of steepening and erosion of electron temperature profile, the plasma develops strong MHD activity. The growth of MHD modes enables further penetration of the impurity gas into plasma core [6]. This resulted in plasma core cooling and the formation of hollow electron temperature profiles (Figure 1). Following this phase the complete plasma energy collapse occurs very quickly.

Unlike the constant gas puff scenario, MGI results in fast penetration (up to 200m/s) of the cooling front into plasma core up to the critical radius of flux surface, triggering fast energy collapse (Figure 2). The temperature profile remained peaked before the energy collapse. The reconstruction of fast magnetic data in JET gives $l_i = 0.6\text{-}0.7$ for both types of disruptions indicating a flattering of the current density profile. Simulation of the process of plasma current flattening indicates that strong electric fields (up to 20V/m) are induced inside the current inversion radius. Simplified analysis predicts that such values are high enough to enable RE generation (Dreicer), which together with hot-tail generation during fast plasma cooling creates the initial population of seed RE that is eventually amplified by secondary generation. In the same time range the plasma enters into current quench (CQ) stage.

5. CURRENT QUENCH AND RE GENERATION

Runaway electrons generated during CQ produced photo-neutrons and HXR emissions. HXR emission has been measured using NaI(Tl) and BGO spectrometers. Each recorded HXR spectrum can be characterised by the average energy $<T_{HXR}>$ and the maximal energy E_{MAX} (Figure 3). It was possible to measure the integral spectrum of RE during the entire plateau duration. New fast data acquisition system allowed measurements of HXR spectra in different time ranges during CQ and RE plateaux.

The HXR raw data measured by BGO spectrometer has been processed using de-convolution procedure (in detail see [10]). This procedure allowed reconstruction of the spectrum of generated RE. Reconstructed RE spectra revealed the increase of maximal energy of RE and indicated the presence at least of two populations of RE electrons with different mean energies (Figure 4). Average and maximal energies of the recorded spectra revealed the expected increasing trend with the decrease of characteristic e-folding time of CQ (Figure 5). This dependence, in general, corresponds well with theory, since the lower values of characteristic e-folding time of CQ correspond to the higher plasma current time derivatives and hence higher electric fields.

However, time-resolved measurements of the HXR spectra during CQs and plateaux have demonstrated more complicated dependencies in RE generation process (Figure 6). In this figure the average and maximum energies are plotted versus the time after beginning of CQ.

Measurements of HXR spectra have been carried out in at chosen time points during the CQ and

plateau stages. To reduce the errors, the data was integrated over a time-interval of several msec. In order to interpret the evolution of the RE energy versus time the following mechanisms should be considered. The first known process is that the enhanced loss of RE at the beginning of CQ (large MHD) does not allow to RE gain high energies at large time derivatives of plasma currents (~200MA/sec) [10]. The measured energies (E_{MAX} up to 7MeV) are too low in comparison to values expected from: $\gamma = \sqrt{(1+(e / mc \cdot \int E_{||0}(t)dt)^2)}$ ~50-60 (for electric field at 50V/m, which is acting during 0.002sec). From another hand, they are too high if the MHD induced high RE losses are considered. Note, that usually plasma current decay lasts about 3-7msec before the RE plateaux formed [6]. The first data points in Figure 6 were obtained within 3-5msec of CQ after the main MHD activity that triggers the disruption. The question arises, why long time after MHD activity phase electrons are not able to be accelerated in the presence of electric fields of 50 V/m. A second process, often underestimated, influences the RE generation.

The plasma energy collapse and re-arrangement of plasma current distribution lead to uncontrolled fast motion of the plasma during the CQ (e.g. problem of plasma control during the fast energy loss). Usually during the CQ the plasma column at JET moves predominantly inward when limiter configurations are used in experiments (most often used for RE experiments), and/or vertical in the case of diverted configurations. In a majority of past studies [4,9,12,13] it was assumed that the main changes in magnetic energy of plasma column are associated with the current quench (large dI_p/dt), while at the same time the changes in the total inductance (L_p) are small and could be disregarded in the energy conservation equation for plasma current loop circuit in tokamaks:

$$I_p^2 \cdot R_p + \frac{d}{dt}\left(\frac{L_p \cdot I_p^2}{2}\right) = 0 \Rightarrow \quad \pi R_0 E_{||0}(t) + L_p \frac{dI_p}{dt} + 0.5 \cdot I_p \frac{dL_p}{dt} = 0 \qquad (1)$$

As a result, the electric field term used in simulations of RE generation depends only on dI_p/dtt [4,9,14]. However, due to fast changes of plasma geometry and corresponding variations of the plasma total inductance $L_p = \mu_0 \cdot R_0 \cdot (\ln(8R_0/a_p) + l_i/2–2)$, the term containing dI_p/dt is not small and may be of opposite sign to dIp/dt [15]. For example, the plasma moves towards inner limiter in disruption Pulse No: 63117 with velocity ~90m/s [6]. No measurable signatures of RE generation were observed during this move. One can calculate that inward motion of the plasma current carrying channel with such velocity will result in $dL_p/dt = 4\times10^{-4}$ H/s in a tokamak with $R_0 = 3$ m and $a_p = 1$m [15]. In this case, is still not high enough to generate large RE energies even dI_p/dt ~200MA/sec.

Therefore, the equation (1) in complete form should be used to calculate the electric field. The end of the inward radial motion coincides well with the appearance of the RE plateaux. Note, vertical plasma motions have larger detrimental effect on RE plateaux stability decreasing their duration.

After achieving the maximum in measured energies, the RE energy starts to decrease. This process should be associated to the current substitution effect, which decreases the electric fields on RE plateau according to:

$$E_{||}(t) = E_{||0}(t)\left(1 - j_{RE} / (j_{pl} + j_{RE})\right)$$

Analysis of the induction of the electric field and RE generation after disruptions, taking into account constraining effects of plasma column geometry evolution [15] have shown strong amelioration of RE generation in the presence of horizontal and/or vertical plasma motions. Moreover, the evolution of the MGI triggered disruption #77982 (Figure 7) demonstrates the prompt RE generation on CQ in the absence of noticeable plasma dynamics along major radius (except small move at thermal quench (TQ).

The data on HXR and soft X-ray emissions collected during long lasting RE plateaux of MGI disruptions enabled the study of spatial and temporal evolution of RE beams. Tomographic reconstructions of HXR and SXR have been carried out (Figure 8 and 9). Both reconstructions reveal complicated emission shapes, which are gradually changing in time.

SXR reveals an evolution from the hollow to quasi-flat distributions. Apparently, the presence of a large amount of injected gas enabled the observation of SXR images of RE beams in-flight. Interaction of RE beam with PFC in JET (indicated by the bright SXR spots near inner wall in Figure 8) can cause a current peeling effect. This effect should extend the current plateaux due to generation of an additional flux time derivative when certain amount of current is lost to the wall according to:

$$\Delta I_p(t) = \int_0^{a(t)} (j_p(r,t)+j_{RE}(r,t)) \cdot 2\pi r dr - \int_{r(t)}^{a(t)} (j_p(r,t)+j_{RE}(r,t)) \cdot 2\pi r dr \qquad (3)$$

The HXR tomography shows at least two spatially distinguished regions in the RE beam cross-section. Bright spot is in the core, which disappears during plateau, and outer hollow toroid, which gradually increases its brightness during plateau. An image of the toroid has crescent-like form due to the lack of HXR channels viewing inner part. Both evolutions indicate that spatial structures of RE beams are more complicated that it was considered early [4,12].

Yet another new phenomenon was discovered during HXR measurements of RE plateaux. Spectrometer with vertical LoS detected the appearance of a second peak in HXR emission growing with the increase of RE plateaux duration in argon MGI triggered disruptions (Figure 10). The constant gas puff scenario did not reveal any measurable HXR emission (Pulse No: 79424, Figure 10). It is likely, that reliable measurements of HXR are linked to interaction of RE beams with surrounding gas in case of MGI [5]. Interaction of the RE and the wall also should contribute into HXR emissivity.

7. RE BEAM IMPACT ONTO PFC IN JET

Formation of nested toroidal layers with different RE current densities inside the plasma column has been analysed in several simulations of the evolution of primary generation and secondary avalanching of RE [9,13,14]. In experiments [4] this phenomenon has been associated with observation of rapid decreases in RE plateaux and bursts of photo-neutrons, HXR and SXR (loss of the current sheets onto PFC). Dependence of photo-neutrons bursts amplitude ($\Delta\Gamma_n$) measured

by 3 detectors on the values of lost RE current (negative part of diagram) is presented in Figure 11 (red, grey and magenta squares). In argon MGI disruptions the RE plateaux revealed sudden rises with simultaneous intense bursts of photo neutrons, SXR and HXR and with following time decay. The dependence of photo-neutrons bursts (from all 3 detectors, black, green and blue circles) on the RE currents increase is shown in the positive part of diagram of Figure 11.

Several effects resulting in emission of electrons at interaction of energetic electrons with the surface of PFC are known. To study the possibility to generate electrons with parameters high enough to contribute to the total RE current at interaction of RE with PFC in JET the numerical simulations using Monte-Carlo code ENDEP have been carried out [16]. Processes associated with Compton and inverse Compton effects, as well as Auger and photoelectric effects are included in the code. It calculated the ratio Iresult/Iimpact between the number of RE impacting on a surface (Iimpact) and number of RE (Iresult) released from PFC surface after interaction for typical single JET CFC tile.

Mono-energetic RE beams and the RE flux with the spectrum E=exp(-E/E0) have been simulated (Figure 12). L is the wetted area along the tile surface. The ratio of the transverse energy Etr to full energy E is taken Etr/E = 0.002. For Etr/E>0.005 the absorption of the incident RE is greater than generation, similarly for mono-energetic RE with E=4 MeV. However, the simulation yielded a certain range for parameters of plasma-born RE at which an additional generation of secondary RE from the surface of PFC is possible.

8. FIRST ANALYSIS OF DISRUPTIONS IN JET WITH ILW

The first JET operations with ITER-like Wall (ILW) have demonstrated that this new environment does not favour to the RE generation after major disruptions. Electron temperatures were measured of about 100 eV or more at the start of the CQ. Observed CQs were more than 10 times slower than those at CFC resulting in lower accelerating electric fields (Figure 13). Moreover, high plasma temperatures, densities and lower impurity levels (Z) also affected the threshold field for runaway generation.

SUMMARY

The enhanced capabilities of JET diagnostics provided new contributions to the physical model of runaway electrons generated by disruptions, in support to development of disruptions mitigation techniques for ITER.

2D tomography of hard and soft-X emissions enabled detailed study of the spatial structure and time evolution of RE beams on plateau stage. The maximum energies of RE populations in some disruptions achieved 15 MeV.

A new phenomenon is discovered: the appearance and gradual increase of a temporal secondary maximum of HXR emission in combination with an increase of RE current plateaux duration. Monte Carlo simulation have confirmed the possibility of the secondary RE generation at interaction of the existing RE fluxes with plasma facing components in JET

ACKNOWLEDGEMENT

This work was supported by EURATOM and carried out within the framework of the European Fusion Development Agreement and of the Contract of Association between the EURATOM and Instituto Superior Tecnico and has also received financial support from Fundação para a Ciência e Tecnologia (FCT), Portugal. The views and opinions expressed herein do not necessarily reflect those of the European Commission.

REFERENCES

[1]. ITER Physics Basis. Chapter 3: MHD stability, operational limits and disruptions 1999 Nuclear Fusion **39** 2137

[2]. T.C. Hender et al. ITER Physics Basis chapter 3: MHD stability, operational limits and disruptions, 2007 Nuclear Fusion **47** 128–200

[3]. S. Putvinski et al. 1997 Plasma Phys. Control. Fusion **39** B157

[4]. R.D. Gill et al. 2002 Nuclear Fusion **42** 1039

[5]. V Riccardo et al. 2010 Plasma Physics and Controlled Fusion **52** 124018

[6]. V.V. Plyusnin et al. 2006 Nuclear Fusion **46** 277

[7]. C. Reux et al 2010 Nuclear Fusion **50** 095006

[8]. M. N. Rosenbluth and S. V. Putvinski 1997 Nuclear Fusion **37** 1355

[9]. L.-G. Eriksson et al. 2004 Physical Review Letters **92** 205004

[10]. A. Shevelev et al. This conference, report ITR/P5-36

[11]. M. Lehnen et al. 2011 Nuclear Fusion **51** 123010

[12]. A. Loarte et al. 2011 Nuclear Fusion **51** 073004

[13]. S. Putvinski et al. 1997 Journal of Nuclear Materials **241-243** 316

[14]. H.M. Smith et al. 2009 Plasma Physics and Controlled Fusion **51** 124008

[15]. V.V. Plyusnin & I.M. Pankratov, 2011 38 EPS Conference on Plasma Physics and Controlled Fusion, Strasbourg 2011 report P4.091

[16]. B. Bazylev et al. 2011 Journal of Nuclear Materials **415** S841

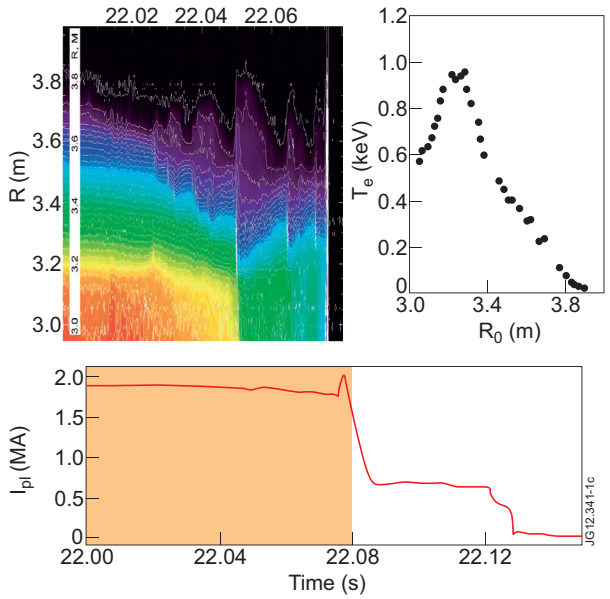

Figure 1: Disruption of Pulse No: 79425. Slow argon injection (activation time is t = 21.5 sec) colored area shows time range of contour plot of $T_e(r,t)$ (upper chart). Last T_e profile (upper chart, left) was measured at t = 22.0758.

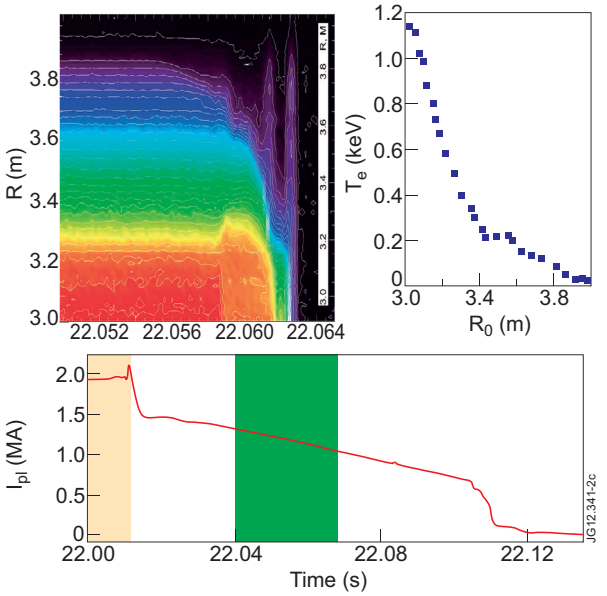

Figure 2: Disruption of Pulse No: 79415. MGI with argon. (DMV activation time is t = 22.05) Marked area after 22.05s shows the time range of $T_e(r,t)$ contour plot (upper chart), T_e profile is taken at 22.0625 s. Green area (after 22.1s) shows range of HXR and SXR measurement (Figures 8 and 9).

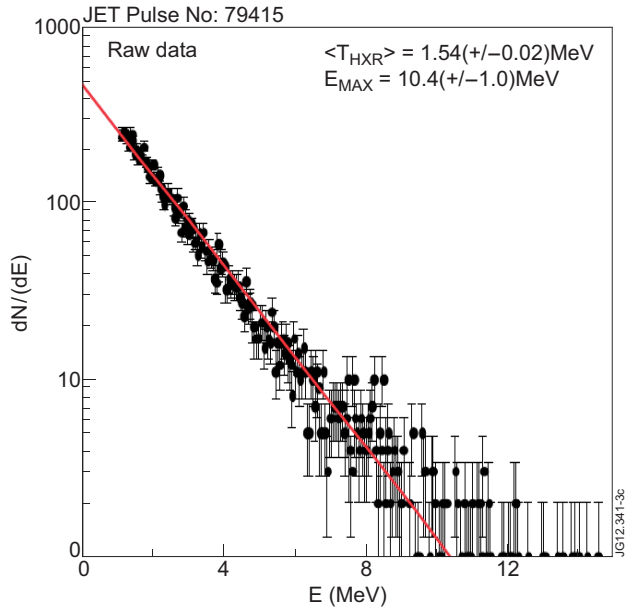

Figure 3: Integral spectrum of HXR recorded using BGO spectrometer in MGI induced disruption.

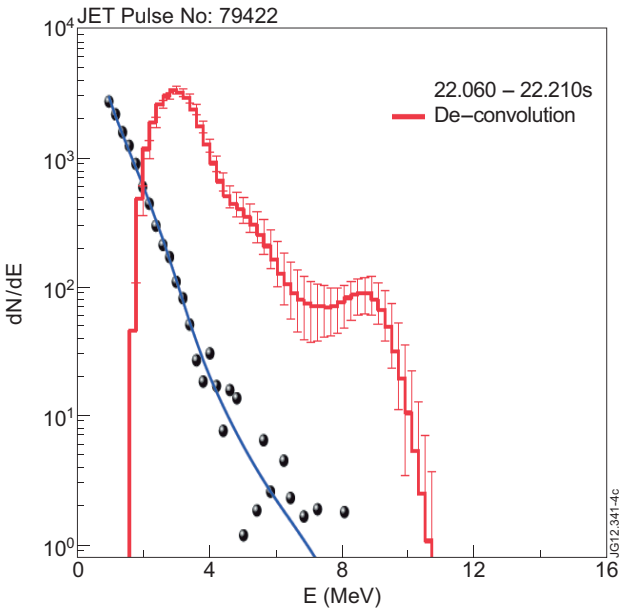

Figure 4: Recorded HXR spectrum (raw data, black circles) in MGI disruption Pulse No: 79422 and reconstructed spectrum of RE obtained using de-convolution procedure (red).

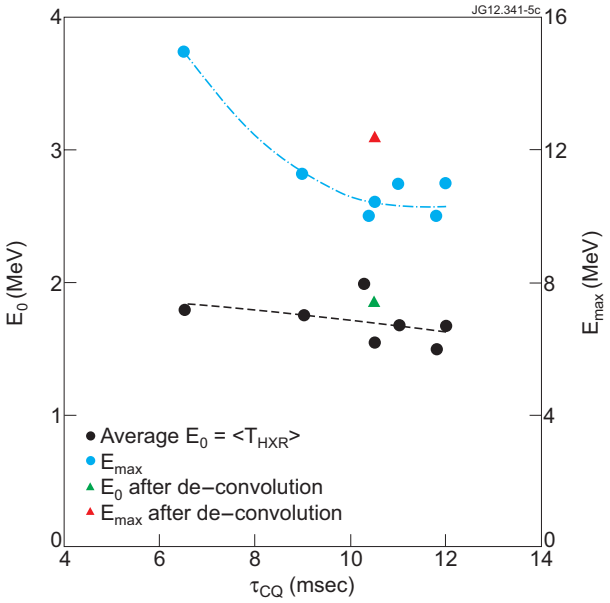

Figure 5: HXR spectrometry. BGO detector. Maximal E_{MAX} and average $E_0 = <T_{HXR}>$ energies versus characteristic e-folding time of CQ.

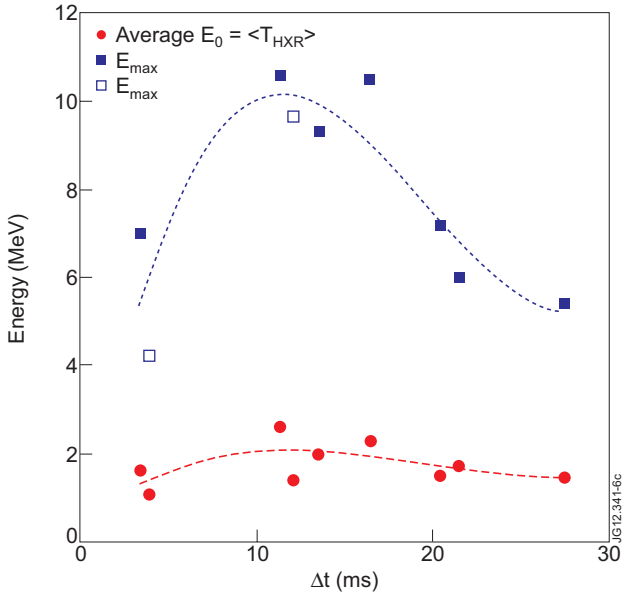

Figure 6: HXR spectrometry. NaI(Tl) detector, fast DAQ, vertical LoS. Maximal E_{MAX} and average $E_0 = <T_{HXR}>$ energies versus time from the beginning of CQ.

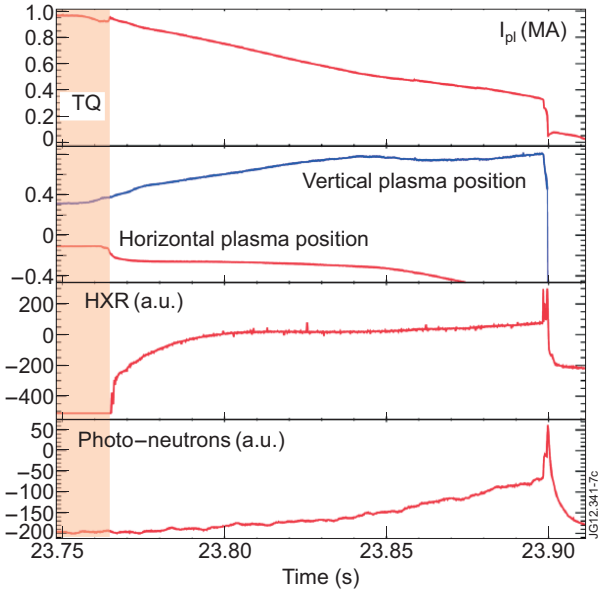

Figure 7: MGI disruption Pulse No: 77982 – low current (<1MA) and prompt RE generation – detected immediately after TQ (end of coloured area).

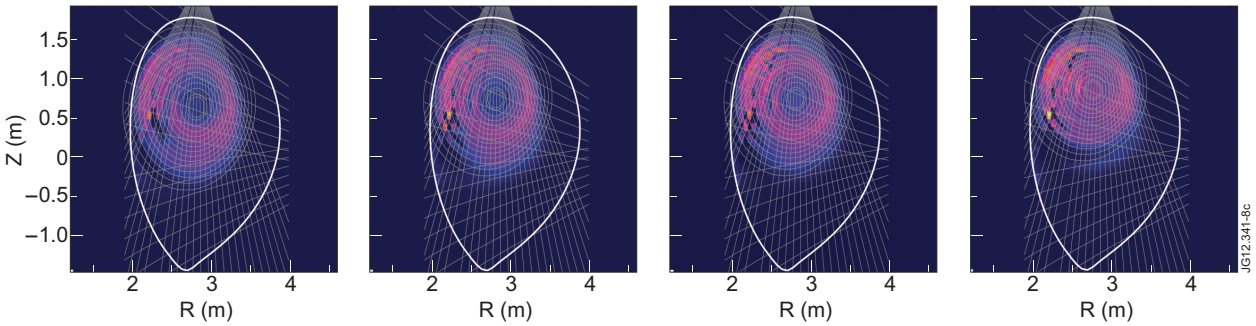

Figure 8: Disruption Pulse No: 79415. SXR tomography of RE plateau. Images produced at t = 22.104, 22.114, 22.124 and 22.134s (e.g. 4ms later than HXR images in Figure 9).

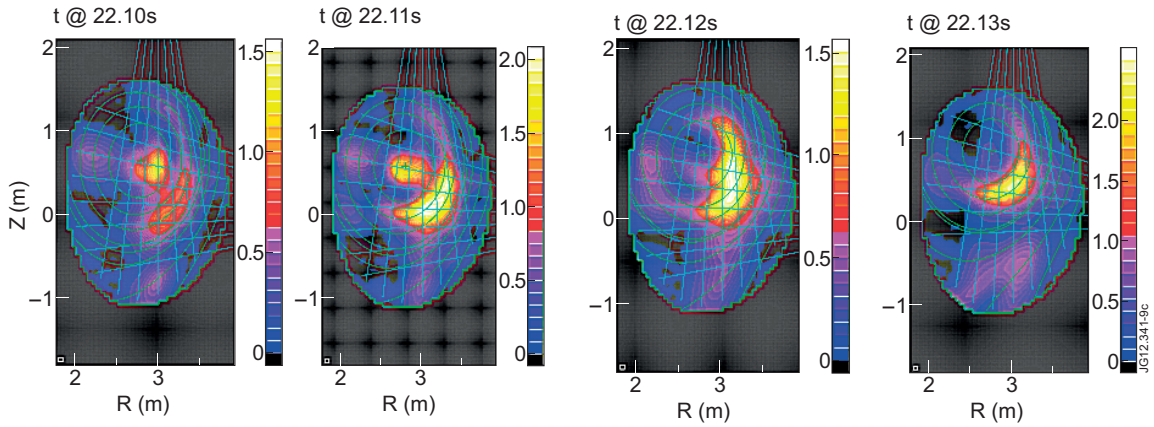

Figure 9: Hard X ray tomography reconstruction of MGI disruption Pulse No: 79415.

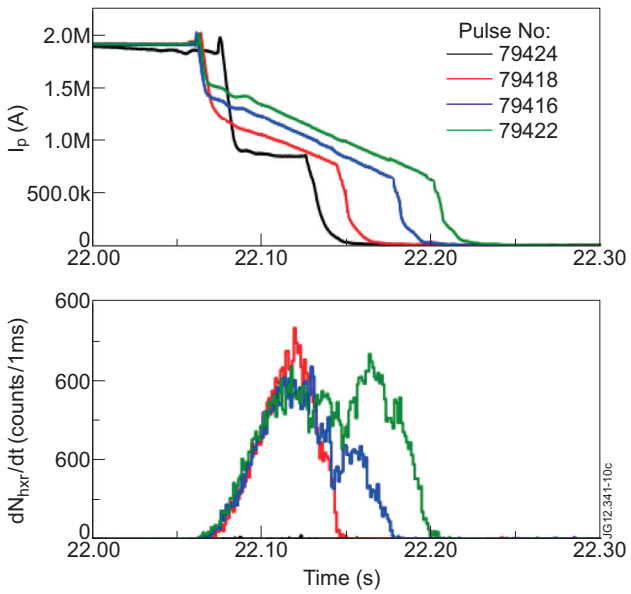

Figure 10: HXR measurements during RE plateaux induced by MGI (Pulse No's: 79416,18,22) and slow gas injection (Pulse No: 79424)

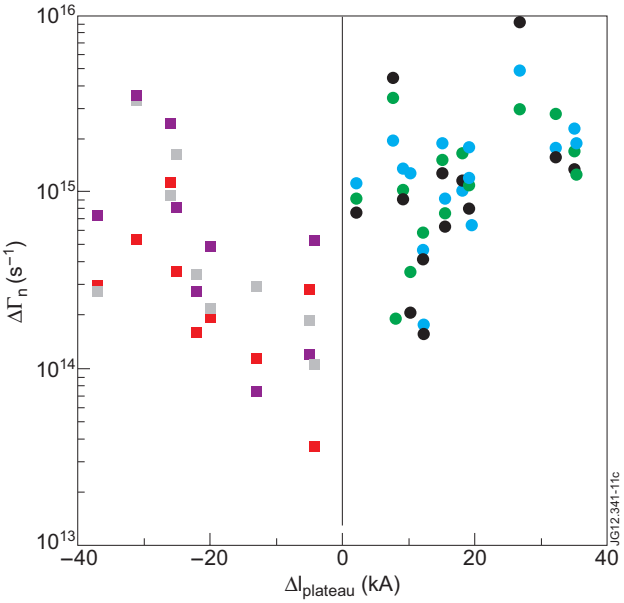

Figure 11: Statistics on neutron bursts $\Delta\Gamma_n$ observed during RE plateau current loss and step-like increases of RE currents.

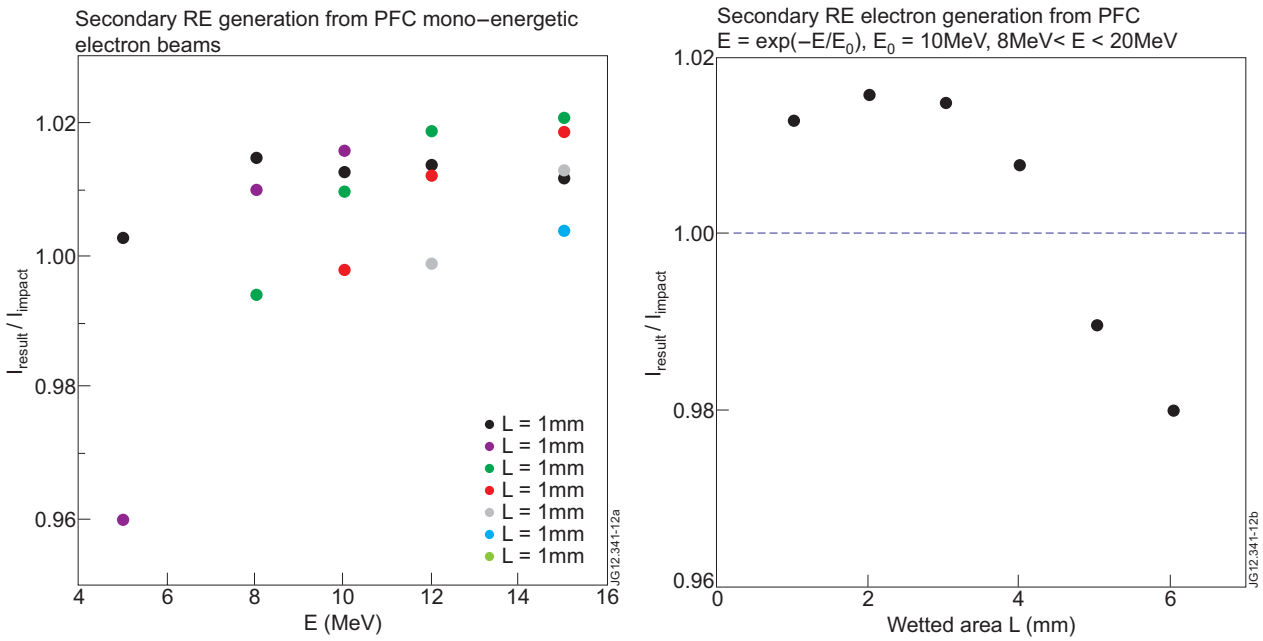

Figure 12: Monte-Carlo simulations for mono-energetic beams (left chart), and for RE flux with E = exp(–E/E_0)) E_0 = 10MeV for energy range 8MeV < E < 20MeV (right).

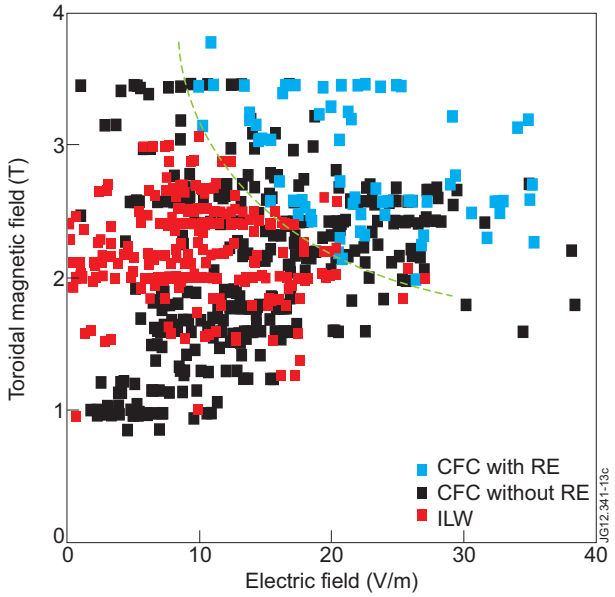

Figure 13. Data map on electric fields generated at CQ in disruptions with CFC and ILW. Data range of RE generation events is bounded by green line.